

Discovery of a new transient X-ray pulsar in the Small Magellanic Cloud

S. Laycock¹, R. H. D. Corbet^{2,3}, D. Perrodin^{2,3}, M. J. Coe¹, F. E. Marshall², and C. Markwardt^{2,4}

¹ Dept. of Physics and Astronomy, University of Southampton, Highfield, Southampton SO17 1BJ, UK
e-mail: sgtl@astro.soton.ac.uk

² NASA Goddard Space Flight Center, Greenbelt, MD 20771, USA

³ Universities Space Research Association

⁴ Department of Astronomy, University of Maryland, College Park, MD 20742, USA

Received 23 August 2001 / Accepted 25 January 2002

Abstract. Systematic *Rossi X-Ray Timing Explorer (RXTE)* observations of the Small Magellanic Cloud (SMC) have revealed a previously unknown transient X-ray pulsar with a pulse period of 95s. The 95s pulsar, provisionally designated XTE SMC95, was detected in three Proportional Counter Array (PCA) observations during an outburst spanning 4 weeks in March/April 1999. The pulse profile is double peaked reaching a pulse fraction of ≈ 0.8 . The X-ray spectrum is well represented by an absorbed power-law with a photon index of 1.4 and mean unabsorbed flux of $\gtrsim 8.95 \times 10^{-11}$ ergs cm⁻² s⁻¹ (3–25 keV). The source is proposed as a Be/neutron star system on the basis of its pulsations, transient nature and characteristically hard X-ray spectrum. The 2–10 keV X-ray luminosity implied by our observations is $\gtrsim 2 \times 10^{37}$ ergs s⁻¹ which is consistent with that of normal outbursts seen in Galactic systems. This discovery adds to the emerging picture of the SMC as containing an extremely dense population of transient high mass X-ray binaries.

Key words. galaxies: Magellanic Clouds – stars: binaries: general – stars: pulsars: general – stars: pulsars: individual: XTE-SMC95 – X-rays: stars

1. Introduction

Observations of the SMC by *RXTE*, *ASCA* & *SAX* have detected an increasing number of new transient X-ray pulsars over the last few years, e.g. Haberl & Sasaki (2000), Yokogawa et al. (2000). With no sign of a decline in this trend, the picture emerging from this flurry of new identifications and rediscoveries of sources seen by *Einstein* and *ROSAT* is that the SMC contains a large population of X-ray binary systems, of which only a small fraction are active at any one time. The SMC provides the closest available approximation to a luminosity-limited sample of X-ray pulsars due to its low extinction and small size. The depth of the SMC is small relative to its distance from us, placing all of the pulsars at effectively the same distance. *RXTE*'s proportional counter array is well suited to studying this population since its field of view, sensitivity and timing resolution allow simultaneous monitoring of all sources in a significant fraction of the SMC.

Observational data from across the spectrum has provided a coherent classification of X-ray binaries, both in

the Galaxy and Magellanic clouds. The principal distinction is between high and low mass stellar counterparts, forming a distinction that is also generally coincident with that between sources exhibiting coherent X-ray pulsations, and those that do not. In high mass X-ray binary (HMXB) systems the optical emission is dominated by the star, while in the latter low mass (LMXB) case, emission from an accretion disk around the compact object dominates. The HMXBs fall into only two subclasses on the basis of their optical classification, those with an OB supergiant (SG) optical counterpart and those involving a Be emission-line star, which account for the majority of HMXBs. These two subgroups broadly coincide with two distinct modes of X-ray behaviour, persistent and transient sources.

Systems containing a supergiant are persistent sources of X-rays which are usually modulated by eclipses due to the short orbital period and correspondingly small size of the system. In very short period systems the primary overfills its Roche-lobe and the overflowing matter is forced by its high angular momentum into a stable accretion disk around the neutron star. In more widely separated systems, persistent emission arises by accretion

Send offprint requests to: S. Laycock,
e-mail: sgtl@astro.soton.ac.uk

from a roughly spherically symmetric stellar wind. Pulse-timing measurements suggest that long-term stable accretion disks do not form in these systems, although short-lived torque-reversals observed in many systems (Bildsten et al. 1997) imply the formation of transient accretion disks.

Transient X-ray sources account for the majority of HMXBs. The neutron star's (NS) optical companion is generally a Be III-V star exhibiting a strong infrared flux excess. Long term monitoring of these systems has resulted in a "standard model" in which the Be star, rotating close to its breakup speed, is surrounded by a dense equatorial disk of cool material. This disk is prone to successive phases of building and ejection on timescales of 1–3 years (Coe 2000). The neutron star, in a wide (few 10 s–100 s of solar radii) eccentric orbit around the Be star, periodically intercepts the ejected material leading to the formation of an accretion disk and X-ray emission. This general model explains the regular X-ray outbursts of Be/NS systems, which are modulated at the orbital period and normally occur close to periastron passage of the neutron star. The situation is complicated by changes in the circumstellar disk which alter the density of material being encountered by the neutron star. This leads to long epochs (several orbital periods) of heightened X-ray activity often accompanied by strong torque reversals and prolonged periods of spin-up. Over the long-term, such activity leads ultimately to a dynamic equilibrium between the orbital and neutron star spin periods since the pulsar experiences negative as well as positive torques. The equilibrium is manifested observationally in the P_{Pulse} vs. P_{Orbit} diagram (Corbet et al. 1999). See also Corbet (1986), Stella et al. (1986) and Bildsten et al. (1997) for detailed explanations.

With the addition of recent discoveries there are now 25 X-ray pulsars known in the SMC. Of these X-ray sources, the majority have been identified as belonging to Be systems rather than supergiant systems (Haberl & Sasaki 2000). Comparing these figures to the population in the Galaxy in which about 70 HMXBs are known, 31 identified with Be optical companions, the SMC emerges as containing a particularly dense population of Be X-ray binaries. Furthermore of the 14 supernova remnants (SNR) identified in the SMC none is Crab-like (Yokogawa et al. 2000). Since Crab-like SNR are believed to form from the explosion of a single massive star it is likely that the evolutionary history of the SMC has resulted in a large ratio of massive binary stars to isolated massive stars. When the comparison is scaled by relative masses of the SMC and Galaxy it is clear that the population density of HMXBs in the SMC is higher even than the Galaxy's most populous regions. Many authors e.g. Staveland-Smith et al. (1997) and Popov et al. (1998) have proposed an evolutionary scenario for the SMC in which an extremely active epoch of star formation occurred relatively recently (within 5 Myr), leading to the large proportion of young, massive stars. In support of this theory are 4 key observations: (1) large number of supernova remnants approximately 5 Myr old; (2) the large number of HMXBs; (3) apparent absence of

low mass systems which would represent an older stellar population (these still remain elusive despite the current generation of satellites' ability to detect them if they are similar to galactic LMXBs); (4) the ratio of Be/B type stars in the SMC is 0.39 (Maeder et al. 1999) compared to 0.16 in the Galaxy, implying a younger population.

2. The RXTE observations

The *RXTE* Proportional Counter Array (PCA) (Jahoda et al. 1996) consists of 5 collimated, Xenon filled, proportional counter units (PCU), each with a collecting area of 1300 cm². The field of view of the PCA is approximately 2°FWZI with a triangular collimator response as a function of off-axis viewing angle. The PCA has 3 detector-anode layers, this arrangement greatly increases the signal/noise by physically separating the detection of low, medium and high energy X-rays. In certain data modes (Good Xenon and Standard 2) this separation is maintained in the telemetry, allowing data from each layer and PCU to be analysed independently. The highest timing and spectral resolution are obtained in Good Xenon mode, in which the energy and arrival time of every detector event is registered with 1 μ s timing accuracy and 256 channel energy resolution. Standard 2 mode provides time-binned data with 16 s resolution and 129 energy channels. Both of these data modes were used in our analysis, as explained in Sect. 3.

RXTE observations were obtained in the course of our regular pulsar search program of the SMC. Approximately every week, 3 ksec observations were made centred on one of 4 partially overlapping positions (see Table 1 and Fig. 1) in the "bar" and "wing" regions of the SMC where young objects are expected to be found (Kahabka & Pietsch 1996) This program began in January 1999 and has allowed detailed monitoring of the long-term behaviour of pulsars in the vicinity of SMC X-3 (Lochner et al. 1999). At the time of the observations presented here, all four pointing positions were being routinely observed, with about three quarters of the time concentrated on the region around SMC X-3 (position 1). However since early 2000 our strategy has changed to allow us to observe the single position centred on SMC X-3 with much greater regularity, since most of the pulsars seen during this program and by *ASCA* (Haberl & Sasaki 2000) have been visible in this position.

Two observations of position 1 taken seven days apart during March 1999 revealed the existence of a transient X-ray pulsar (XTE SMC95) whose 95 s pulse period and pulse profile we were able to determine. The next position 1 observation two weeks later revealed weak pulsations, after which the source faded from view.

Although individual pointed detections of a transient source are unable to constrain its position, the only impact of this positional uncertainty on PCA data analysis is uncertainty in absolute flux determination. Given the high timing resolution and *S/N* typically obtainable for

Table 1. Dates and positions of observations.

Obs. Date	Position	Duration /ks	Source
1 25/2/99	1	2.20	-
2 4/3/99	2	3.38	-
3 11/3/99	1	3.13	XTE SMC95
4 18/3/99	1	3.49	XTE SMC95
5 26/3/99	3	3.76	-
6 1/4/99	1	3.78	XTE SMC95
7 9/4/99	1	4.49	-
8 22/4/99	1	2.98	-

Position 1: RA = 13° 471; Dec = -72° 445, *Position 2:* RA = 16° 25; Dec = -72° 106, *Position 3:* RA = 18° 75; Dec = -73° 091, *Position 4:* RA = 12° 686; Dec = -73° 268 (Equinox 2000.0).

SMC pulsars, this limitation is unimportant in the identification of new sources and the study of pulse profiles and pulse-frequency evolution, which are the primary aims of this program.

3. Data reduction

Good Xenon mode data from the PCA were used to construct lightcurves and spectra. 4 PCUs were active during the observations presented here. In order to maximise signal-to-noise ratio, only events from the top anode layer of each active proportional counter unit (PCU) were included and the analysis was restricted to the 3–25 keV energy range. The PCA is sensitive to X-rays between 2–60 keV, although for faint sources its spectral response seems unreliable below 3 keV. The X-ray flux from pulsars falls off rapidly above 10 keV.

Additional filtering criteria were applied to exclude data collected during periods of high background occurring shortly after SAA passage and short data segments coinciding with start and finish of pointing slews. Background subtraction was performed using the L7 PCA faint background models (gain epochs 3 and 4) provided by the *RXTE* Guest Observer Facility. These models use the Standard 2 mode PCA data to determine various parameters used in estimating the background count-rates and spectra in the specific PCU and anode-layer configuration being used for each observation. Background corrected lightcurves were then constructed at 100 ms timing resolution, with bin times corrected to the solar-system barycentre and the count-rates normalised to counts $\text{PCU}^{-1} \text{s}^{-1}$. A detailed description of the L7 background model is given by Edelson & Nandra (1999).

4. Timing analysis

In order to search for pulsars in the datasets, we calculated power spectra covering a period range 0.1–1000 s at a resolution of 0.1 mHz. Coherent pulsations were initially detected in observation 3 and power spectra showing the positive detection of XTE SMC95 are shown in Figs. 2 and 3. These power spectra show several harmonics of

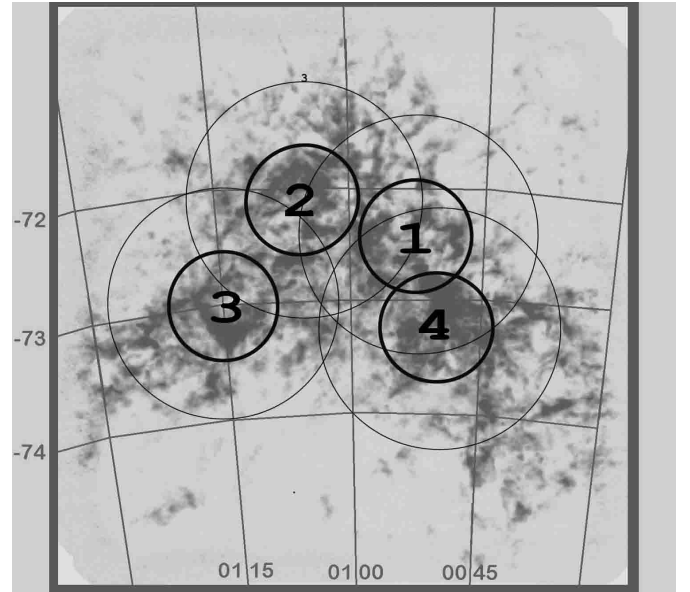


Fig. 1. fields of view used in our systematic monitoring program, superimposed on an H1 radio map of the SMC (Stanimirovic et al. 1999). The precise pointing centres are given in Table 1. The thick and thin circles represent the half-power width and FWZI of the PCA respectively. Data from the 4th position are not presented in this work.

the fundamental spin frequency, whose relative strengths changed between the two observations. The fundamental and harmonic frequencies were weighted by their spectral power to obtain a best fit to the true period. The uncertainty in the period was calculated by propagating the error (FFT resolution) from each harmonic. Two harmonics were used to establish the period in observation 3, three in observation 4 (see Figs. 2 and 3).

After determining the pulse period and associated observational errors, average pulse profiles were created for each of the observations. The profiles are shown in Fig. 4, while key observational parameters derived from them are given in Table 2. The mean fluxes have formal uncertainties of 0.03 counts $\text{PCU}^{-1} \text{s}^{-1}$ before taking into account contribution from interfering sources and uncertainties in the background model. Using observations for our monitoring program in which no pulsations were detected, an estimate was made of the contribution from unpulsed X-ray sources in the field, such as supernova remnants. The mean background corrected 3–10 keV flux averaged over its 3 lowest values for observations of Position 1 is 0.98 ± 0.05 Count $\text{PCU}^{-1} \text{s}^{-1}$ with an excess variance in the count rates of 13% over the expected Poisson level. Thus the true 3–10 keV pulse fraction in observation 3 (see Fig. 4) was ≈ 0.8 .

A weak 95 s pulsation was detected in observation 6, however the flux was dominated by 91 s pulsations from the nearby pulsar AX J0051-722. Due to the closeness of the two pulse periods, direct measurement of the pulse amplitude of SMC95 was not possible. Instead simulated

Table 2. Summary of timing results.

Obs. number	Pulse period seconds	Pulse amplitude [†] Ct PCU ⁻¹ s ⁻¹	Mean flux [†] Ct PCU ⁻¹ s ⁻¹
3	95.49 ± 0.05	2.72 ± 0.26	4.34
4	95.03 ± 0.03	2.27 ± 0.25	4.08
6	95.0 ± 0.1	0.2–1.0*	3.79

[†]Background corrected 3–25 keV. * See Sect. 4.

data sets were created using the pulse profile obtained in observation 4 as a template and varying its pulse amplitude. These simulated data were used to estimate the pulse amplitude required to recreate the 95 s peak seen in the observation 6 PDS. The resulting upper limit (see Table 2) is approximately one third the amplitude seen in obs. 4 and is found to be nearly 10 times the amplitude required if the modulation were sinusoidal, a possibility supported by the lack of harmonics in the PDS. Considering the mean count-rate in the observations, it is clear that most of the flux in observation 6 was due to AXJ0051-722. Thus the brightness of SMC95 is constrained to be in the lower end of the range determined from the timing alone.

5. Spectrum analysis

PCA spectra were obtained from the first two observations containing XTE SMC95, the spectra are well represented by an absorbed power-law typical of Be/X-ray binary pulsars (e.g. White et al. 1983). The fitted model parameters are given in Table 3 for the two observations and are in agreement to within errors. Figure 5 shows the spectrum from observation 4, along with the fitted model and residuals. Uncertainties in the fitted parameters represent the limits of the 90% confidence interval. The unabsorbed source fluxes were obtained from the fitted spectral models. Uncertainties in the absolute flux are dominated by the unknown source position and hence collimator response. Since both observations were made with the same pointing, the uncertainty is systematic.

6. Source location

PCA slew data were used to constrain the source position. The PCA detectors are often on and accumulating data as the spacecraft is manoeuvred on-source during the start of an observation. As the source moves through the collimator field of view, it samples different values of the collimator response function, which modulates the detected count rate. Given a trial position and intensity for the source, a model light curve can be constructed using a tabulated response function, and compared to the observed light curve. The position and intensity are then varied iteratively using least squares fitting until the best-fit parameters are obtained. Ideally, two scans completely over the source are needed, in orthogonal directions, to constrain the source position with the highest precision. When, as

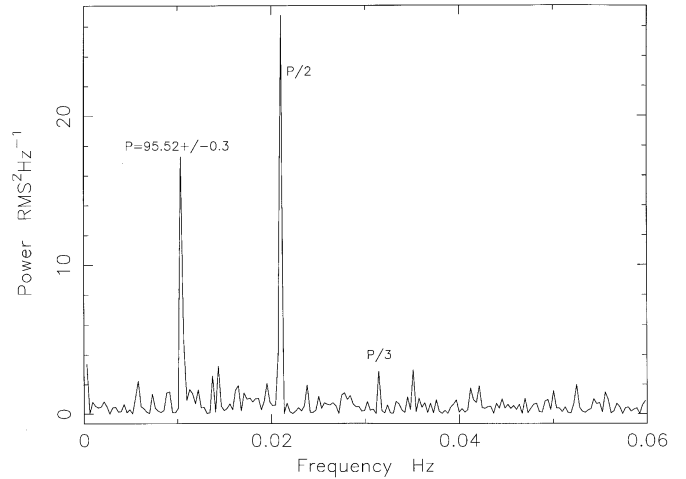


Fig. 2. PCA 3–25 keV power spectrum showing fundamental pulse frequency and harmonics of XTE SMC95 in observation 3.

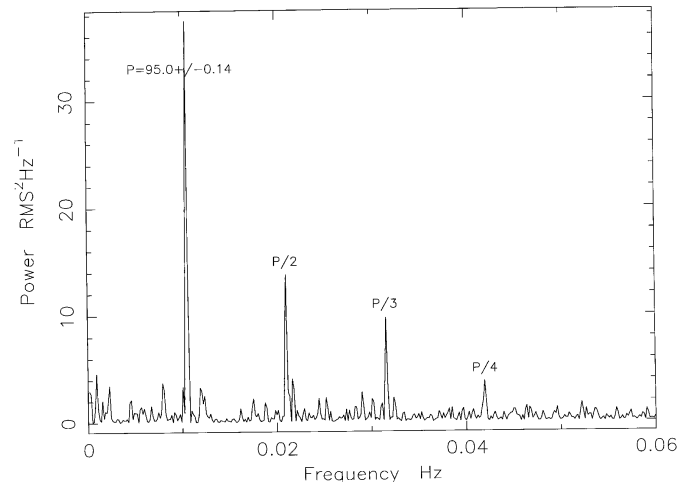


Fig. 3. PCA 3–25 keV power spectrum showing fundamental pulse frequency and multiple harmonics of XTE SMC95 in observation 4.

in this case, the scans are not complete, and not at right angles, the error box will be larger and asymmetric.

Light curves for XTE SMC95 were extracted from the 16-second Standard2 data in the 2–10 keV band (PCA top layer only) for observations 3 and 4. The light curves included approximately 200 s of slewing and on-source time each. The model included a term for the PCA background, which was fixed at the value determined from the PCABACKEST model for faint sources. The intrinsic variability of the pulsar can be confused with variations of source position. To compensate for this, the light curve error bars were increased proportionately by 30% (this number was also scaled according to the collimator response at each time sample). The value of 30% was determined by fitting a constant intensity during the pointed portion of the observation, and forcing $\chi^2_{\nu} = 1$, and represents the effective fractional rms variation of the pulsar on 16 s timescales.

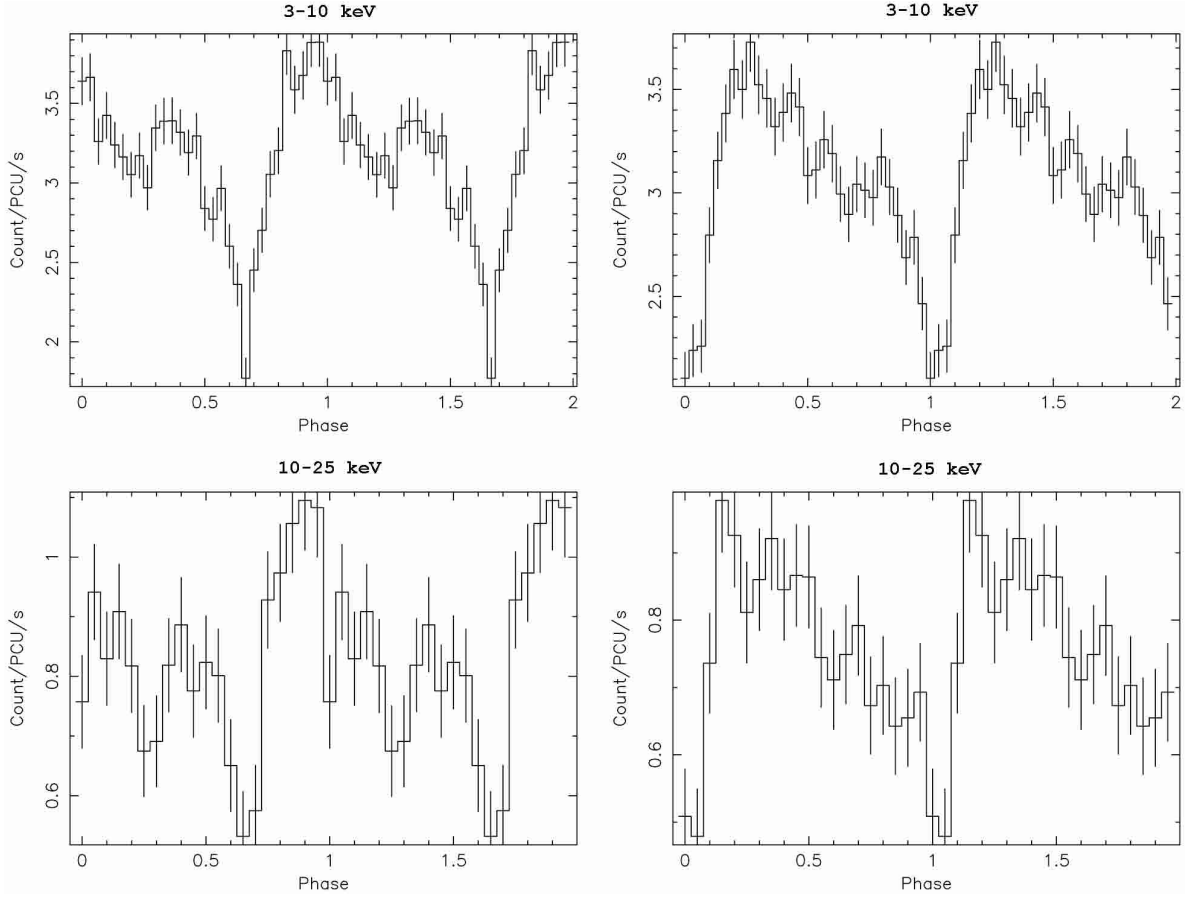


Fig. 4. Pulse profiles for XTE SMC95 in 3–10 keV and 10–25 keV energy bands (arbitrary phase, $T_0 = \text{MJD } 51248$). Left column: observation 3. Right column: observation 4.

Table 3. Spectral fits to observations.

Obs.	N_{H} $\times 10^{22}$	α	flux [†]	L_{X}^{\ddagger}	χ^2_{ν}
3	1.82 ± 0.89	1.41 ± 0.23	8.95	2.14	0.86
4	2.66 ± 0.89	1.50 ± 0.07	8.43	2.15	0.89

[†] Total unabsorbed model flux $\times 10^{-11} \text{ erg cm}^{-2} \text{ s}^{-1}$ (3–25 keV)

[‡] 2–10 keV model luminosity $\times 10^{37} \text{ erg s}^{-1}$ at 63 kpc.

N.B. These are upper limits with a factor ~ 5 uncertainty in flux & L_{X} due to unknown collimator response. (No corrections applied).

χ^2_{ν} for 58 degrees of freedom.

The best fitting position was $\alpha = 13.36^\circ$, $\delta = -72.821^\circ$ (J2000), with a reduced chi-square value of 1.02. The position uncertainty is a thin strip shown in Fig. 6. Confidence contours were estimated by taking $\Delta\chi^2 = 6.2, 9.2, 11.8, 18.4$, which formally represent confidence levels of 2σ , 99%, 3σ , and 99.99% respectively, for two parameters. However, because the variability of the pulsar is non-statistical and non-trivial to model, we favor assigning the 3σ contour as the smallest reasonable error box. The semi-minor and semi-major axes of the error box are 5 arcmin and 41 arcmin respectively. Since

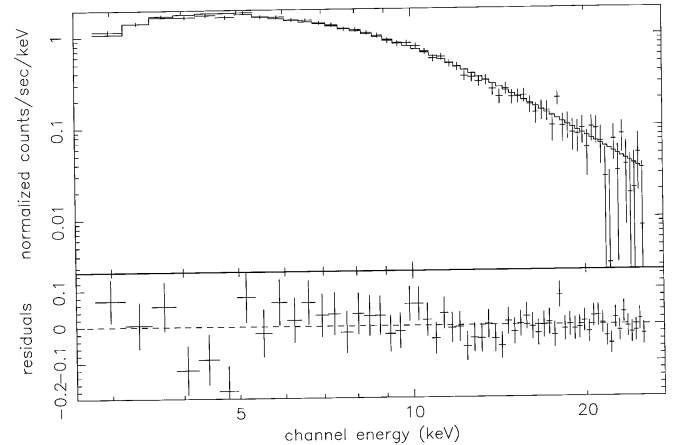


Fig. 5. *RXTE* PCA spectrum obtained during observation 3, when XTE SMC95 was the only detectable pulsar in the field of view. Solid line is an absorbed power-law fit, residuals are shown in the lower panel. See Table 3 for details of the spectral parameters.

the source was not detected in PCA observations at pointing positions number 2 and 4, which are east and south of pointing position number 1, respectively, it is more likely that the source is located to the northwest of the best-fit position.

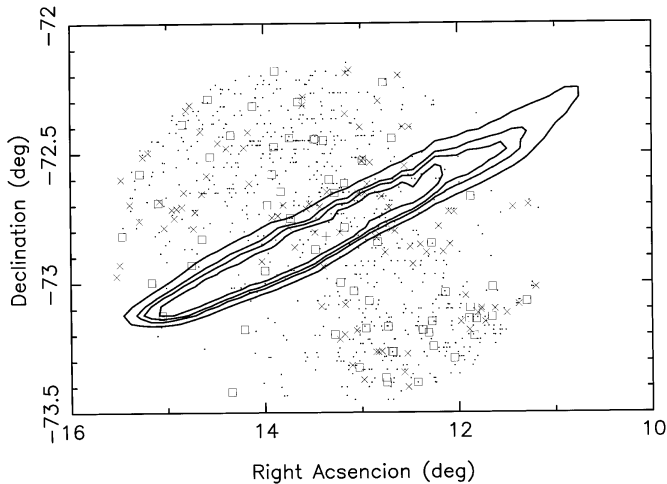


Fig. 6. Confidence contours for the position of XTE SMC95. Formal confidence levels are 2σ , 99%, 3σ , and 99.99% (see Sect. 6). The best fit position is shown as a “+” symbol, and the position of the PCA at pointing position number 1 is indicated with a circle. ROSAT sources are indicated by squares, luminous O/B stars crosses, H α stars dots. See Sect. 8

The true intensity of the source depends on *its position within the PCA collimator response function*. At the best-fit position, the collimator response is $\sim 60\%$, implying that the source is $\sim 65\%$ brighter than implied by the counting rate observed by the PCA at pointing position number 1. Given the full error box described above, the collimator response could potentially be in the range of 10%–75%. If the source is northwest of the best-fit position, the collimator response is in a more restricted range of 60%–75%, and then it is likely that the observed rate is close to the actual source flux, within a factor of ~ 2 .

7. Duration of the outburst

As Table 1 shows, XTE SMC95 was not detected in observations made before and after those presented here. The closest before and after observations were made at pointing positions 2 and 3 respectively, one week either side of the detected outburst. As Fig. 1 shows, these observations provide no useful information due to their limited overlap, other than possibly constraining XTE SMC95 to lie towards the west in the position 1 field of view. The closest position 1 observations occurred within two weeks of the outburst. Analysis of power spectra obtained in these bracketing observations allow us to place upper limits on the X-ray flux during apparent quiescence. From this analysis we find that XTE SMC95 pulse amplitude was below our approximate 3σ detection threshold of 0.25 counts $\text{PCU}^{-1} \text{s}^{-1}$ in observations 1 and 7, where this figure is directly comparable with the measured fluxes in observations 3 and 4.

8. Discussion

Most galactic Be/X-ray binaries increase in luminosity by a factor of $\gtrsim 100$ during normal outburst (Negueruela 1998) reaching luminosities around $10^{37} \text{ erg s}^{-1}$. Taking the distance to the SMC as 63 kpc (Groenewegen et al. 2000), the fluxes given in Table 3 imply a 2–10 keV luminosity for XTE SMC95 of at least $2 \times 10^{37} \text{ erg s}^{-1}$. Thus during this outburst the X-ray luminosity of XTE SMC95 was comparable to that of Galactic Be/NS systems. The photon indices obtained from our spectral fits are slightly steeper than those normally seen in Galactic Be/NS HMXBs, values $\lesssim 1.0$ being typical in the 10–20 keV range (White et al. 1983). Softer (steeper) spectra have been associated with less luminous sources based on studies in the Galaxy (White et al. 1983). Comparing our results (Table 3) to the recent outburst of SMC X-2 which was both more luminous and had a harder spectrum: luminosity $\approx 10^{38} \text{ erg s}^{-1}$, spectral index 0.7–1.0 (Corbet et al. 2001) this trend looks likely to hold in the SMC.

XTE SMC95 exhibited varying structure in its pulse profile. Pulse profiles obtained in two separate energy bands 3–10 keV and 10–20 keV shown in Fig. 4 indicate the pulse-shape changed between the two observations (3 and 4), with the second pulse peak weakening relative to the first, accompanied by a decrease in pulsed flux. The significant shift in relative strength of the first and second power spectrum harmonics between the two observations (see Figs. 2 and 3) confirms that the profile change is real and not an artifact of an incorrect profile-folding period.

A small decrease in the pulse period was detected between the two observations of XTE SMC95 one week apart, implying a pulse period derivative $(8.6 \pm 5.5) \times 10^{-7} \text{ s s}^{-1}$. This change is attributed to an unknown combination of spin up and orbital motion depending on the inclination of the system.

For Be/NS systems with P_{pulse} around 95 s, the Corbet diagram (Corbet 1986) suggests likely orbital periods in the 50–100 d range. XTE SMC95 was detected for three weeks, only a small fraction of its likely orbital period. Whether this outburst was related to orbital motion or long-term changes (disk-loss events) in a circumstellar disk may be determined by continued monitoring.

A search of ROSAT catalogues of the SMC (Kahabka et al. 1999, Haberl et al. 2000), reveals 4 sources within the 3σ confidence region (see Fig. 6). Of these sources, RX J0053.8-7252 and RX J0052.6-7247 are possible candidates and lie within 4 arcmin of the best-fit position. The other sources are a supersoft X-ray source and a foreground star. All 4 sources appear in Kahabka et al. (1999), only RX J0052.6-7247 and the foreground star appear in Haberl et al. (2000). A similar search for known Be stars was made in the same region. Searching the AzV (Azzopardi & Vigneanu 1982) & LIN (Lindsay 1961) catalogues for spectral types: O8-B2, I-V, gave 7 stars within the 3σ contour. This range of spectral types was chosen to match the known distribution for optical counterparts to HMXBs (Negueruela 1998). The AzV catalogue is 80%

complete to limiting magnitude $B = 14.3$, considering the distance to the SMC the sample is strongly biased toward early-type giants. Thus main sequence Be stars (luminosity class IV-V) are likely to be under represented in the sample. The catalogue of $H\alpha$ emission-line objects of Meyssonnier & Azzopardi (1993) lists 69 stars within the 3σ contour. From the argument given above, the majority of these are likely to be O/Be stars.

Acknowledgements. We thank the referee, W. Heindl for constructive comments. This research has made use of the SIMBAD database, operated at CDS, Strasbourg, France. SL is supported by a PPARC studentship.

References

- Azzopardi, M., & Vigneanu, J., A&AS, 50, 291
 Bildsten, L., Chakrabarty, D., Chiu, J., et al. 1997, ApJS, 114(2)
 Buckley, D. A. H., Coe, M. J., Stevens, J. B., et al. 2001, MNRAS, 320, 281
 Coe, M. J. 2000, ASP Conf. Ser., 214, ed. M. A. Smith, H. F. Henrichs, & J. Fabregat, 656
 Coe, M. J., Buckley, D. A. H., Negueruela, I., et al. 2000, HEAD 32.2302C
 Corbet, R. H. D. 1986, MNRAS, 220, 1047
 Corbet, R. H. D., Marshall, F. E., Peele, A. G., & Takeshima, T. 1999, ApJ, 517, 956
 Corbet, R. H. D., Marshall, F. E., Coe, M. J., Laycock, S., & Handler, G. 2001 ApJ, 548, L41
 Edelson, R., & Nandra, K. 1999, ApJ, 514, 682
 Finger, M. H., Wilson, R. B., & Harmon, B. A. 1996, ApJ, 459, 288
 Groenewegen, M. A. T. 2000, A&A, 363, 901
 Haberl, F., Filipovic, M. D., Pietsch, W., & Kahabka, P. 2000, A&AS, 141, 41
 Haberl, F., & Sasaki, M. 2000, A&A, 359, 573
 Jahoda, K., Swank, J. H., Stark, M. J., et al. 1996, Proc.SPIE, 2808, 59
 Kahabka, P., & Pietsch, W. 1996, A&A, 312, 919
 Kahabka, P., Pietsch, W., Filipovic, M. D., & Haberl, F. 1999, A&AS, 136, 81
 Lindsay, E. M. 1961, AJ, 66, 169
 Lochner, J. C., Whitlock, L. A., Corbet, R. H. D., & Marshall, F. E. 1996, A&AS, 194, 5218
 Maeder, A., Grebel, E. K., & Mermilliod, J. C. 1999, A&A, 346, 456
 Meyssonnier, N., & Azzopardi, M. 1993, A&AS, 102, 451
 Negueruela, I. 1998, A&A, 338, 505
 Popov, S. B., Lipunov, V. M., Prokhorov, M. E., & Postnov, K. A. 1998, Astron. Rep., 42, 29
 Santangelo, A., Cusumano, G., dal Fiume, D., et al. 1998, A&A, 338, L59
 Stanimirovic, S., Staveley-Smith, L., Dickey, J. M., Sault, R. J., & Snowden, S. L. 1999, MNRAS, 302, 417
 Staveley-Smith, L., Sault, R. J., Hatzidimitriou, D., Kesteven, M. J., & McConnell, D. 1997, MNRAS, 289, 225
 Stella, L., White, N. E., & Rosner, R. 1986, ApJ, 308, 669
 White, N. E., Swank, J. H., & Holt, S. S. 1983, ApJ, 263, 277
 Yokogawa, J., Imanishi, K., Tsujimoto, M., et al. 2000, ApJS, 128, 491